



# Interaction of cyanidin-3-O-glucoside with three proteins



Tang Lin\*, Li Shu, Bi Hongna, Gao Xin

School of Life Science, Shandong Normal University, Jinan, PR China

## ARTICLE INFO

### Article history:

Received 20 April 2015

Received in revised form 4 August 2015

Accepted 23 September 2015

Available online 28 September 2015

### Keywords:

Cyanidin-3-O-glucoside

Hemoglobin

Myoglobin

Bovine serum albumin

Spectroscopic

Molecular modeling

## ABSTRACT

We studied the binding of cyanidin-3-O-glucoside (C3G) with bovine serum albumin (BSA), hemoglobin (Hb) and myoglobin (Mb), using multi-spectral techniques and molecular modeling. Fluorescence and time-resolved fluorescence studies suggested that C3G quenched BSA, Hb or Mb fluorescence in a static mode with binding constants of 4.159, 0.695 and  $1.545 \times 10^4 \text{ L mol}^{-1}$  at 308 K, respectively. The thermodynamic parameters represented hydrogen bonds and van der Waals forces dominated the binding. Furthermore, CD, UV-vis, and three-dimensional fluorescence spectra results indicated the secondary structures of BSA, Hb and Mb were partially destroyed by C3G with the  $\alpha$ -helix percentage of C3G-Hb and C3G-Mb decreased while that of C3G-BSA was increased. UV-vis spectral results showed these binding interactions partially affected the heme bands of Hb and Mb. In addition, molecular modeling analysis supported the experimental results well. The calculated results of equilibrium fraction showed that the concentration of free C3G in plasma was high enough to be stored and transported from the circulatory system to reach their target sites to provide their therapeutic effects.

© 2015 Elsevier Ltd. All rights reserved.

## 1. Introduction

Anthocyanins, a group of water-soluble flavonoids subgroup, are widely distributed in fruits and vegetables, but also found in flowers and other plant materials. They are responsible for red, blue and purple colours (Fleschhut, Kratzer, Reckemmer, & Kulling, 2006). The most common naturally occurring anthocyanins are the 3-O-glucosides and the 3,5-O-diglucosides of malvidin, cyanidin, pelargonidin, delphinidin, petunidin and peonidin (Fleschhut et al., 2006). Cyanidin-3-glucoside (C3G), a typical representative of anthocyanins in food, is widespread in plants (Fig. 1). There are several reports mentioning its beneficial effects. For example, cyanidin-3-glucoside (C3G) exhibits free radical scavenging activity, suppresses inflammation, protects against endothelial dysfunction, vascular failure and myocardial damage, prevents obesity, ameliorates hyperglycemia and seems to help prevent cardiovascular disease (Kähkönen & Heinonen, 2003; Noda, Kaneyuki, Mori, & Packer, 2002; Seeram, Momin, Nair, & Bourquin, 2001; Serraino et al., 2003; Tsuda, Horio, Uchida, Aoki, & Osawa, 2003; Xu, Ikeda, & Yamori, 2004). In order to be transferred into a tumor, C3G needs to be bound by various proteins after ingestion, so knowing the details of the binding characteristics of C3G with

these proteins in the therapeutic procedure at molecular level is of great importance (Xie et al., 2014).

Proteins are important biomacromolecules that play various roles in living beings (Mahato et al., 2010). Serum albumin is the most abundant drug carrier protein in blood plasma, which has many physiological functions, such as maintaining the osmotic pressure and pH of blood, and as carriers transporting a great number of endogenous and exogenous compounds such as fatty acids, amino acids, drugs and pharmaceuticals (Kratz, 2008). Thus, bovine serum albumin (BSA) was selected as a model protein. Hemoglobin (Hb) and myoglobin (Mb) are proteins which could involve in redox activities. They play an important role in physiological activities in human bodies, having numerous functions including the transport of oxygen, dispersion of hydrogen peroxide, and are involved in electron transfer reactions (Chen, Ikeda-Saito, & Shaik, 2008; Cheng, Liu, Bao, & Zou, 2011). Hb picks up oxygen from the tiny blood capillaries at the base of the lungs and carries it along the arteries to the body tissues, and carries CO<sub>2</sub> from the cells to the lungs for removal (Chatterjee & Kumar, 2014). Mb is found mainly in muscle tissues, and receives oxygen from red blood cells and transports it to the mitochondria of the muscle cells, where the oxygen is used in cellular respiration to generate energy. Hb is a tetrameric protein comprising of four polypeptide chains: two identical  $\alpha$ -chains comprising of 141 amino acid residues each and two identical  $\beta$ -chains made up of 146 amino acid residues, while Mb is a single polypeptide chain protein of 153 amino acids (Chatterjee & Kumar, 2014). Although

\* Corresponding author at: College of Life Science, Shandong Normal University, 88 East Wenhua Road, Jinan, Shandong Province 250014, PR China.

E-mail address: [tanglin@sndu.edu.cn](mailto:tanglin@sndu.edu.cn) (L. Tang).

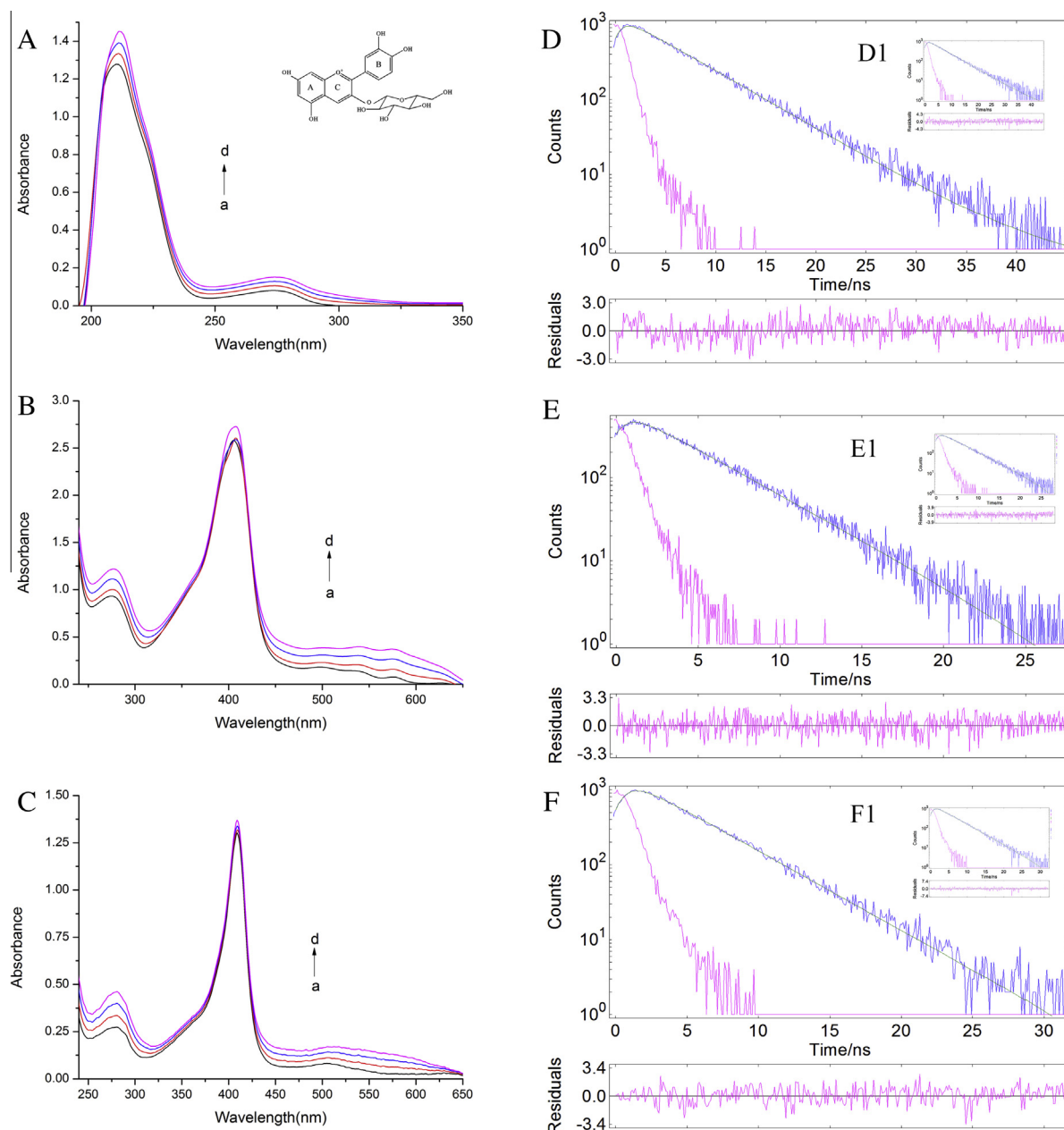


**Fig. 1.** Chemical structures of cyanidin-3-O-glucoside, UV absorption spectra of BSA (A), Hb (B) and Mb (C) without and with C3G.  $c(\text{BSA}) = 2.0 \mu\text{mol L}^{-1}$ ,  $c(\text{C3G})/c(\text{BSA}) = 0-3$ .  $c(\text{Hb}) = c(\text{Mb}) = 10.0 \mu\text{mol L}^{-1}$ ,  $c(\text{C3G})/c(\text{Hb}) = 0, 0.1, 0.2, 0.5$ ,  $c(\text{C3G})/c(\text{Mb}) = 0, 0.1, 0.2, 0.5$ . Fluorescence decay profiles and residual fit for BSA (D, D1), Hb (E, E1) and Mb (F, F1) ( $55 \mu\text{mol L}^{-1}$ ) in the absence and presence of C3G ( $2 \mu\text{mol L}^{-1}$ ).

Hb and Mb are not strictly plasma proteins, investigations on the interaction of drugs and small molecules with Hb and Mb are of great importance in terms of understanding their pharmacological actions.

Till now, most reports have focused on anthocyanins (Fleschhut et al., 2006; Kähkönen & Heinonen, 2003; Tang, Zuo, & Shu, 2014). However, to our best knowledge, the interactions of C3G with BSA, Hb and Mb have not been reported. Therefore, it is necessary to understand the level of binding of C3G with BSA, Hb and Mb, which will directly correlate with the efficiency of C3G *in vivo*.

The objective of this study is to investigate the *in vitro* binding characteristics of C3G with three proteins using multispectral and molecular modeling techniques. The multiple spectroscopic techniques include ultraviolet (UV)-visible absorption spectroscopy, time-resolved fluorescence, synchronous fluorescence

spectroscopy, three-dimensional fluorescence spectra and circular dichroism (CD) techniques. These results could provide more detailed information to understand the delivery process of C3G *in vivo*.

## 2. Experimental

### 2.1. Materials

Bovine serum albumin, hemoglobin from bovine blood and myoglobin from equine heart were all purchased from Sigma Chemical Company (St. Louis, USA), and used without further purification. The cyanidin-3-O-glucoside with purity 95% was purchased from Extrasynthese (Genay, France). Tris with purity over

99% was purchased from Amresco. All other materials were of analytical grade and water used in all experiments was doubly distilled water.

Tris–HCl buffer (0.05 mol L<sup>-1</sup>, pH 7.4) contained 0.10 mol L<sup>-1</sup> NaCl aiming to keep pH and ionic strength. BSA, Mb and Hb were all prepared with Tris–HCl buffer to get the stock solution (1 × 10<sup>-5</sup> mol L<sup>-1</sup>). BSA would be diluted to obtain the working concentration (2 × 10<sup>-6</sup> mol L<sup>-1</sup>) with buffer solution, while working concentrations of Mb and Hb were the same as the stock solution (1 × 10<sup>-5</sup> mol L<sup>-1</sup>). C3G was dissolved in anhydrous ethanol to get the stock solution (1 × 10<sup>-3</sup> mol L<sup>-1</sup>). All the solutions were stored in refrigerator at 4 °C.

## 2.2. Apparatus

All fluorescence spectra were recorded on a Varian Cary Eclipse fluorescence spectrometer equipped with a 10 mm path-length quartz cell. Time-resolved fluorescence measurements were performed using a time correlated single photon counting system from FL920P spectrometer (Edinburgh Instruments, UK). The UV absorption spectra were recorded on a Thermo Scientific NanoDrop 2000C UV–Vis spectrometer equipped with a 10 mm path-length quartz cell. The circular dichroism (CD) spectral data was obtained on a Chirascan Circular Dichroism Spectrometer (Applied Photo-Physics) equipped with a 1 mm path length cell. The pH value was measured using a pH-meter (Shanghai INESA Scientific Instrument Co. Ltd. pH-3D). A micropipettor (Thermo) and electronic balance (OHAUS, Discovery) were used in the experiment.

## 2.3. Fluorescence quenching measurements

The BSA concentration was kept at 2 × 10<sup>-6</sup> mol L<sup>-1</sup>, while Mb and Hb were set at 1 × 10<sup>-5</sup> mol L<sup>-1</sup>. A 3 ml portion of proteins were titrated by continuous additions of 1.0 × 10<sup>-3</sup> mol L<sup>-1</sup> C3G, respectively, to get final concentrations from 1.0 × 10<sup>-6</sup> mol L<sup>-1</sup> to 1.0 × 10<sup>-5</sup> mol L<sup>-1</sup> for C3G. The excitation and emission slit widths were fixed at 5 nm. The excitation wavelength was set at 280 nm and the emission wavelength was recorded in the range of 290–450 nm. The experiment was operated at three different temperatures, 288 K, 298 K and 308 K. The BSA synchronous fluorescence spectra were scanned from 250 to 330 nm ( $\Delta\lambda = 15$  nm) and from 200 to 350 nm ( $\Delta\lambda = 60$  nm), respectively. The excitation wavelength was set at 250–400 nm ( $\Delta\lambda = 15$  nm) and 230–400 nm ( $\Delta\lambda = 60$  nm) respectively for Hb, while that was set at 250–350 nm ( $\Delta\lambda = 15$  nm) and 230–450 nm ( $\Delta\lambda = 60$  nm) for Mb. All the synchronous fluorescence experiments were carried out at 308 K, pH 7.4.

For BSA and Mb, the three-dimensional fluorescence spectrum was performed under the following conditions: the initial excitation wavelength was set at 200 nm with increments of 5 nm and the emission wavelength was recorded between 200 and 450 nm. The three-dimensional fluorescence spectrum of Hb was performed under the following conditions: emission wavelengths at 280–470 nm, excitation at 220 nm with an increment of 5 nm, excitation and emission slit widths was 5/5 nm respectively.

## 2.4. Time-resolved fluorescence experiments

Time-resolved intensity decays of three proteins (5.5 × 10<sup>-5</sup> mol L<sup>-1</sup>) with and without the addition of C3G (2.0 × 10<sup>-6</sup> mol L<sup>-1</sup>) were measured, using a time correlated single photon counting system from FL920P spectrometer (Edinburgh Instruments, UK), operating at 280 nm. Pulse periods of 100 or 50 ns were used as the excitation source. To optimize the signal-to-noise ratio, 10<sup>3</sup> or 5 × 10<sup>2</sup> photon counts were collected in the peak channel. The decay curves were analyzed using the FAST

software package from Edinburgh Instruments. Intensity decay curves were fitted as a sum of exponential terms (Molina-Bolívar, Galisteo-González, Ruiz, Medina-O, & Parra, 2014):

$$I(t) = \sum_i A_i \exp\left(-\frac{t}{\tau_i}\right) \quad (1)$$

where  $\tau_i$  are the decay times,  $A_i$  is a pre-exponential factor for the component  $i$  with a lifetime  $\tau_i$ . The quality of the fits were determined by both chi-squared ( $\chi^2$ ) values and weighted residuals. Average fluorescence lifetimes ( $\tau$ ) were calculated from the two-component contributions using the following equation (Molina-Bolívar et al., 2014):

$$\tau = \frac{\sum_i A_i \tau_i^2}{\sum_i A_i \tau_i} \quad (2)$$

The relative concentration, or fractional amount of each component ( $\alpha_i$ ), was determined by:

$$\alpha_i = \frac{A_i}{\sum_i A_i} \quad (3)$$

## 2.5. UV–vis absorption spectroscopy

A 3 ml portion of proteins were titrated by continuous additions of 1.0 × 10<sup>-3</sup> mol L<sup>-1</sup> C3G, respectively, while the concentration of proteins was the same as fluorescence quenching measurements. The UV–vis absorption spectroscopy was recorded in the range of 190–700 nm at 308 K and the slit width was set at 2.0 nm.

## 2.6. CD spectra

The CD method was used to analyze the structural change of proteins before and after the addition of C3G, using a Chirascan Circular Dichroism Spectrometer equipped with 0.1 cm quartz cells. The recorded CD spectra ranged from 200 nm to 250 nm and the concentration of proteins was 2 × 10<sup>-6</sup> mol L<sup>-1</sup>, while the C3G was 4 × 10<sup>-6</sup> mol L<sup>-1</sup>.

## 2.7. Molecular modeling study

For molecular docking, the BSA molecule model (PDB ID: 3V03), Hb molecule model (PDB ID: 2MHB), Mb molecule model (PDB ID: 1MBS) and C3G model (MI ID: 28426) were used for ligand docking. Docking simulations were performed using AUTODCK4.2 and the Lamarckian genetic algorithm was applied to calculate the possible conformation of the ligand molecule and macro-molecule. The population size of the docking experiment was set as 100. The conformer with the lowest binding free energy was used for further analysis.

# 3. Results and discussion

## 3.1. UV–vis absorption spectra

The structural information of proteins can often be presented by using UV–vis absorption spectra. Unlike BSA, beside the polypeptide chain, heme groups also exist in Hb and Mb (Wang, Zhang, & Cao, 2014). Fig. 1 displays the recorded UV–vis absorption spectra of BSA, Hb or Mb in both the absence and presence of C3G. The results clearly show that BSA, Hb or Mb have two absorption peaks. For BSA, it is obvious that there is a strong absorption peak at around the wavelength of 208 nm and a shoulder peak at 278 nm, which represent the absorption of BSA's characteristic polypeptide backbone structure —C=O and amino acid residues, respectively (Shen, Gu, Jian, & Qi, 2013). For Hb or Mb,

the absorption peak in the region 250–300 nm arises from the transition of  $\pi \rightarrow \pi^*$  in the phenyl groups in tryptophan (Trp), tyrosine (Tyr) and phenylalanine (Phe), in Hb or Mb (Wang, Tang, Zhang, Zhou, & Zhang, 2009). In addition, the peak at about 410 nm is called the Soret band and is the characteristic peak of heme proteins, which can be attributed to the electronic transition of  $\pi \rightarrow \pi^*$  of hematomorph in Hb or Mb (Mahato et al., 2010). The spectral changes of these peaks can reflect the polypeptide backbone structural change, the microenvironment of aromatic acid residues of proteins, or the conformational change near the heme moiety in Hb or Mb. The intensity of these peaks all changed in the presence of C3G compared to the UV–vis absorption spectra of the three proteins in the absence of C3G. The increase of the peaks at 208 and 278 nm, and red shifting of the maximum peak positions of the complexes, indicated BSA's polypeptide backbone had changed after C3G addition and the hydrophobicity of the microenvironment of aromatic amino acid residues increased (Li, Zhu, Jin, & Yao, 2007). The increase of the peak in the region 250–300 nm of Hb or Mb implied micro-environmental changes of aromatic acid residues. Furthermore, the red shift meant more aromatic acid residues were extended into the aqueous environment. In addition, the absorption spectra of the Soret band of Hb and Mb in the presence of C3G also showed spectral changes, but not obviously. Such a phenomenon observed in the absorption spectra of Hb or Mb suggested that C3G interacted with the surface of Hb or Mb, and had no direct effect on its interior structure. The results were consistent with Xie et al. (2014). In a word, these observations strongly suggested that binding interactions existed between C3G and BSA, Hb or Mb. But the decrease of the Hb Soret band was more obvious than that of Mb. We conjectured the reason might be that it is more difficult for C3G enter into Mb than Hb because Hb consists of two  $\alpha$  and two  $\beta$  subunits while Mb is a single chain heme protein.

### 3.2. The fluorescence quenching mechanism

Proteins emit intrinsic fluorescence mainly due to Trp, Tyr and Phe residues. Actually, the intrinsic fluorescence of BSA is mostly contributed by Trp residues alone (Shen et al., 2013). Hb contains three Trp units ( $\alpha$ -Trp 14,  $\beta$ -Trp 15 and  $\beta$ -Trp 37) in each  $\alpha$  and  $\beta$  chain, while Mb contains two Trp residues (Trp 7 and Trp 14) (Wang et al., 2014). Supplementary Fig. 1 shows the fluorescence emission spectra obtained for BSA, Hb or Mb at pH 7.40 with the addition of C3G. It can be seen that the maximum emission wavelength of BSA, Hb and Mb was all around 340 nm with the excitation at 280 nm. It can also be seen that the fluorescence intensity of BSA, Hb and Mb decreased in the presence of C3G, which indicated that C3G might interact with all three proteins. When the concentration of C3G reached  $10 \mu\text{mol L}^{-1}$ , the intrinsic fluorescence of BSA decreased 29.5%, Hb decreased 25.2%, while that of Mb decreased 28.3%. This result implied that the binding strength of BSA was largest among three proteins.

Fluorescence quenching can be dynamic (resulting from collisional encounters between the fluorophore and the quencher) or static (resulting from the formation of a ground-state complex between the fluorophore and the quencher). Static quenching is controlled by forming a complex substance, so with the increasing temperature the static quenching constant will decrease due to the lower stability of the complex, while the opposite effect will be considered as dynamic quenching (Zuo, Tang, Li, & Huang, 2015). In order to distinguish the quenching mechanism, temperature experiments were carried out. They are usually analyzed according to the equation of Stern–Volmer: (Chamani, Vahedian-Movahed, & Saberi, 2011)

$$F_0/F = 1 + K_q \tau_0 [Q] = 1 + K_{SV} [Q] \quad (4)$$

where  $F_0$  and  $F$  are the fluorescence intensities in the absence and presence of the C3G, respectively.  $K_{SV}$  is the Stern–Volmer quenching constant,  $K_q$  is the quenching rate constant of biological macromolecule,  $[Q]$  is the concentration of the C3G,  $\tau_0$  is the life time of the fluorescence in absence of C3G and  $\tau_0 = 10^{-8}$  s.

The results are shown in Table 1 and Supplementary Fig. 2. As shown in the results, the  $K_{SV}$  of the proteins have an opposite tendency with increasing temperature and the values of  $K_q$  were greater than the limiting diffusion rate constant of the biopolymer ( $2 \times 10^{10} \text{ M}^{-1} \text{ s}^{-1}$ ), which indicated that the probable quenching of three proteins between C3G follow the static quenching mechanism (Shen et al., 2013).

In addition, fluorescence lifetime was measured to obtain additional information on the quenching mechanism of the three proteins fluorescence by C3G. The tri-exponential fitted decay curves are shown in Fig. 1, corresponding to BSA without and with the addition of C3G (D and D1), Hb without and with the addition of C3G (E and E1) and Mb without and with the addition of C3G (F and F1). The proteins were excited at 280 nm and the emission intensities were collected at 340 nm. The data required bi-exponential decay functions to achieve an adequate fit with  $\chi^2$  for individual data ranging from 1.0 to 1.1. The average fluorescence lifetimes for BSA alone, and in the presence C3G, were  $\tau_0 = 5.577$  ns and  $\tau = 5.607$  ns, respectively. And that for Hb were  $\tau_0 = 4.040$  ns and  $\tau = 3.953$  ns while the values were  $\tau_0 = 4.110$  ns and  $\tau = 4.055$  ns for Mb. As can be seen, there was no significant change in the fluorescence lifetime when C3G was added to the three proteins, which was indicative of a static quenching mechanism (Patel et al., 2015). The results were consistent with the fluorescence experiment.

### 3.3. Determination of binding parameters and thermodynamic parameters

The binding constant and number of binding sites in the ligand–protein complex were calculated by a double logarithmic curve equation:

$$\log[(F_0 - F)/F] = \log K_a + n \log [Q] \quad (5)$$

where  $K_a$  is the binding constant of the interaction between quenchers and protein and  $n$  is the number of binding sites per protein. The value of  $K_a$  and  $n$  can be acquired by the plot of  $\log[(F_0 - F)/F]$  versus  $\log [Q]$ . The binding constants  $K_a$  and binding sites  $n$  are shown in Table 2. It can be seen from the table that the number of binding sites was close to 1, manifesting that there was a single binding site on BSA, Hb or Mb for C3G. The  $K_a$  values of BSA and Mb were larger than that of Hb, which indicated that the binding affinity of BSA and Mb were stronger than Hb, which was consistent with the fluorescence quenching results. Results also showed that the values of  $K_a$  decreased with increasing temperature, implying that the complex of C3G with BSA, Hb and Mb became unstable with the rising temperature (Wang et al., 2014).

**Table 1**  
Quenching constants of the interaction between C3G and BSA/Hb/Mb.

Compound	T (K)	$K_{SV}$ ( $10^4 \text{ L mol}^{-1}$ )	$K_q$ ( $10^{12} \text{ L mol}^{-1} \text{ s}^{-1}$ )	$R^2$	S.D.
BSA	288	5.773	5.773	0.9996	0.032
	298	4.015	4.015	0.9999	0.025
	308	3.931	3.931	0.9999	0.035
Mb	288	5.327	5.327	0.9998	0.058
	298	4.769	4.769	0.9999	0.035
	308	4.332	4.332	0.9999	0.021
Hb	288	4.351	4.351	0.9998	0.062
	298	4.093	4.093	0.9999	0.054
	308	3.348	3.348	0.9998	0.021



**Table 2**

Binding constants and thermodynamic parameters of BSA/Hb/Mb–C3G systems at different temperatures.

Compound	T (K)	$K_a$ ( $10^4$ L mol $^{-1}$ )	$n$	$R^2$	S.D.	$\Delta H$ (kJ/mol)	$\Delta G$ (kJ/mol)	$\Delta S$ (J/mol/K)
BSA	288	21.581	1.114	0.9952	0.056	–85.30	–29.41	–194.05
	298	6.532	1.043	0.9904	0.004		–24.47	
	308	4.159	1.007	0.9906	0.007		–25.53	
Mb	288	25.119	1.137	0.9910	0.043	–128.45	–29.76	–342.66
	298	4.140	0.989	0.9948	0.009		–26.34	
	308	1.545	0.915	0.9801	0.025		–22.91	
Hb	288	1.589	0.912	0.9730	0.047	–49.95	–23.18	–92.94
	298	0.794	0.985	0.9948	0.063		–22.25	
	308	0.695	0.994	0.9937	0.036		–21.32	

The interaction forces between C3G and proteins often include hydrogen bonds, hydrophobic effects, electrostatic interactions and van der Waals forces. The enthalpy change ( $\Delta H$ ), entropy change ( $\Delta S$ ) and free energy change ( $\Delta G$ ) were evaluated by using Van't Hoff equation

$$\ln K_a = -\Delta H/RT + \Delta S/R \quad (6)$$

$$\Delta G = \Delta H - T\Delta S \quad (7)$$

where  $\Delta H$ ,  $\Delta G$  and  $\Delta S$  are enthalpy change, free enthalpy change and entropy change, respectively.  $R$  is the gas constant 8.314 J mol $^{-1}$  K $^{-1}$  and  $T$  is the temperature.  $K_a$  represents the binding constant at a corresponding temperature. The values of  $\Delta H$ ,  $\Delta G$  and  $\Delta S$  at different temperatures obtained are shown in Table 2. The values of  $\Delta G$  in these binding processes are negative, indicating the spontaneity of the binding of C3G with BSA, Hb or Mb. As for  $\Delta H$ , the values of them were –85.30 kJ mol $^{-1}$ , –128.45 kJ mol $^{-1}$  and –49.95 kJ mol $^{-1}$  for BSA–C3G, Hb–C3G and Mb–C3G, respectively, implying that these binding processes are enthalpy driven. According to Ross's research, when  $\Delta H > 0$ ,  $\Delta S > 0$ , hydrophobic effects are the main force; when  $\Delta H < 0$ ,  $\Delta S < 0$ , van der Waals forces and hydrogen bonds help a lot in the interaction; when  $\Delta H < 0$ ,  $\Delta S > 0$ , it is the electrostatic forces (Ross & Subramanian, 1981). In this work, the negative values of  $\Delta H$  and  $\Delta S$  suggested that hydrogen bonds and van der Waals forces played major roles in the interaction of C3G and BSA, Hb or Mb.

#### 3.4. Energy transfer from BSA, Hb or Mb to C3G

FRET is a distance dependent interaction in which excitation energy is transferred nonradiatively from donor to acceptor. The energy transfer effect is related not only to the distance between the acceptor (protein) and donor (C3G)  $r$ , but also to the critical energy transfer distance ( $R_0$ ), by Förster's non-radiative energy transfer theory: (Shaikh, Seetharamappa, Kandagal, Manjunatha, & Ashoka, 2007)

$$E = 1 - \frac{F}{F_0} = \frac{R_0^6}{R_0^6 + r^6} \quad (8)$$

$$R_0^6 = 8.8 \times 10^{-25} K^2 n^{-4} \Phi J \quad (9)$$

$$J = \frac{\sum F(\lambda) \varepsilon(\lambda) \lambda^4 \Delta \lambda}{\sum F(\lambda) \Delta \lambda} \quad (10)$$

where  $E$  and  $r$  are the energy transfer efficiency and distance between donor and acceptor,  $R_0$  is known as the critical distance when the transfer efficiency is 50%.  $F_0$  and  $F$  are fluorescence intensities of the energy donor in the absence and presence of an energy receptor.  $K^2$ ,  $\Phi$ ,  $n$  and  $J$  are the spatial orientation factor, fluorescence quantum yield of the donor, refractive index of the medium and effect of the spectral overlap integral between the donor

emission and the acceptor absorption, respectively.  $F(\lambda)$  expresses the fluorescence intensity of the donor at the wavelength  $\lambda$ , and  $\varepsilon(\lambda)$  is the absorption coefficient of the energy receptor at the wavelength  $\lambda$ . Here the donor and acceptor were BSA, Hb or Mb and C3G, respectively. The spectral overlaps of the fluorescence emission spectrum of proteins and the absorption spectrum of C3G are shown in Supplementary Fig. 3 and the values are shown in Supplementary Table 1. For BSA,  $K^2 = 2/3$ ,  $n = 1.336$  and  $\Phi = 0.15$ . According to Supplementary Fig. 3 and Eqs. (8)–(10), the values obtained were  $J = 1.03 \times 10^{-15}$  cm $^3$  L mol $^{-1}$ ,  $R_0 = 1.75$  nm,  $E = 0.065$  and  $r = 2.52$  nm. For Hb,  $K^2 = 2/3$ ,  $n = 1.36$  and  $\Phi = 0.06$ , the values obtained were  $J = 3.50 \times 10^{-15}$  cm $^3$  L mol $^{-1}$ ,  $R_0 = 2.14$  nm,  $E = 0.23$  and  $r = 2.62$  nm. Under the same conditions, the values obtained were  $J = 3.55 \times 10^{-15}$  cm $^3$  L mol $^{-1}$ ,  $R_0 = 2.15$  nm,  $E = 0.27$  and  $r = 2.53$  nm. The values of  $r$  were all smaller than 7 nm and  $0.5R_0 < r < 1.5R_0$ , indicating that it would be highly possible that energy transfer from proteins to C3G occurred (Zhou, Lü, Su, Shan, & Chen, 2012). Besides, the donor-to-acceptor distance is within the range of 2–8 nm, which again elucidates a static quenching mode of the system (Lu et al., 2011).

#### 3.5. Synchronous fluorescence analysis

The measurements of synchronous fluorescence spectra are frequently used to indicate the impact of ligands on the conformation of proteins. When the wavelength intervals  $\Delta\lambda$  are kept at 15 or 60 nm, synchronous fluorescence provides the characteristic information of tyrosine residues or tryptophan residues, respectively (Tang et al., 2014). The results are shown in Supplementary Fig. 4. With a gradual addition of C3G, fluorescence intensity of the three proteins decreased. The  $\lambda_{\max}$  of BSA and Mb shifted inconspicuously by addition of C3G as well as the shape of the wave, which illustrated that the binding of C3G to BSA and Mb had little influence on the polarity of microenvironment near the aromatic amino acid residues. The results showed that the maximum emission bands of Hb had an obvious red shift from 290 to 293 nm (see Supplementary Fig. 4C) when the value was set at 15 nm, which indicated that the conformation of Hb had been changed and the polarity around the Trp residues of the protein increased. It also demonstrated that the Trp residues were brought to a more hydrophilic environment (Shen et al., 2013). When  $\Delta\lambda$  was 60 nm, the shifts of the maximum emission bands were unobservable, which meant that the binding of C3G to Hb had little influence on the polarity of microenvironment near Tyr residues.

#### 3.6. Three-dimensional fluorescence spectra

To have a further knowledge about the conformational change of C3G to BSA, Hb or Mb, three-dimensional spectroscopy was investigated on the proteins and protein–C3G complex. It is well-known that three-dimensional fluorescence spectra can provide more detailed information about the configuration of proteins

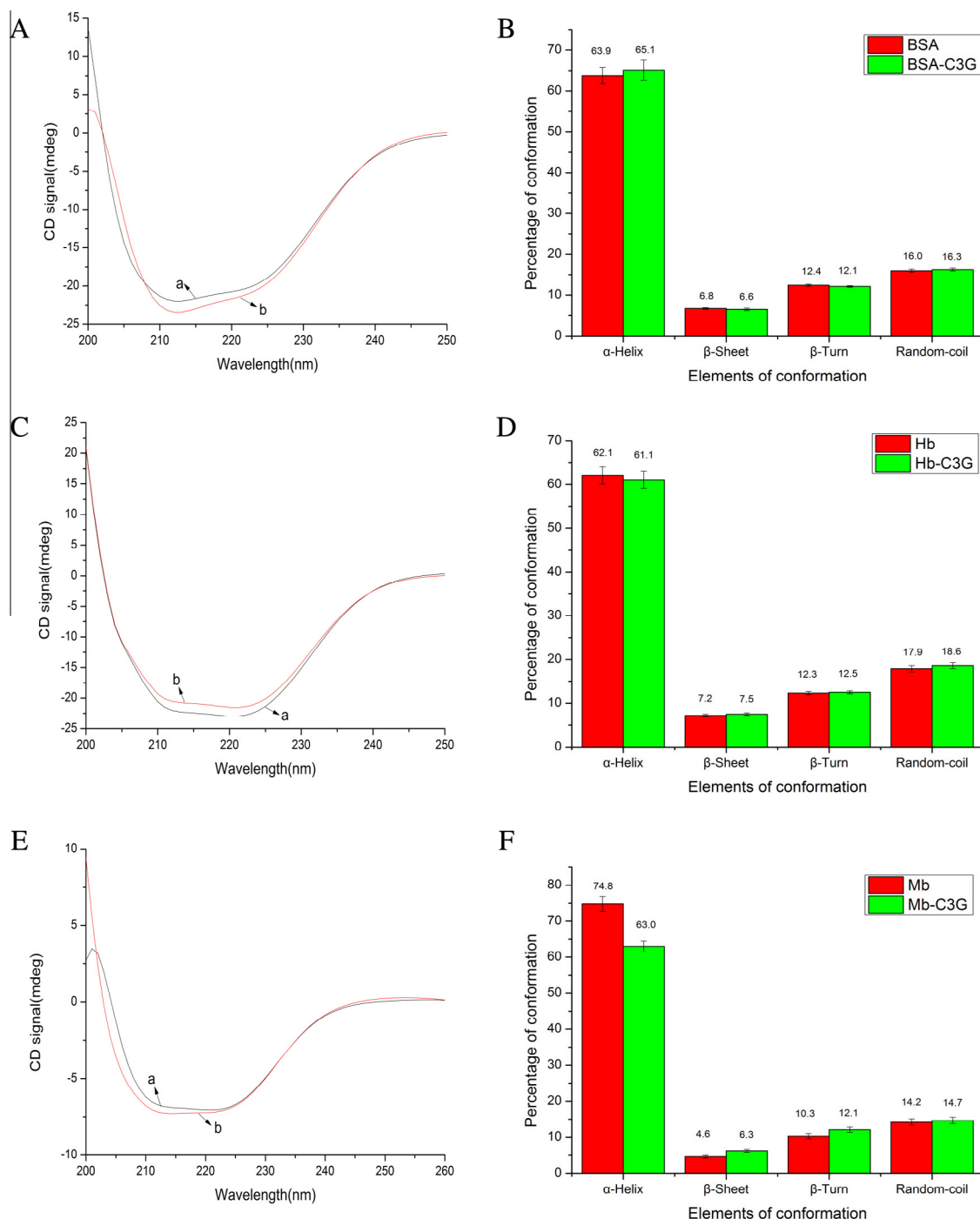


**Fig. 2.** CD spectra of BSA (A), Hb (C) and Mb (E) and bar diagrams of BSA (B), Hb (D) and Mb (F) in the absence and presence of C3G.  $c(\text{BSA}) = 2.0 \mu\text{mol L}^{-1}$ ,  $c(\text{Hb}) = c(\text{Mb}) = 10.0 \mu\text{mol L}^{-1}$ ,  $c(\text{BSA})/c(\text{C3G}) = (\text{Hb})/c(\text{C3G}) = (\text{Mb})/c(\text{C3G}) = 1:2$ .

(Xiang & Wu, 2010). The three-dimensional fluorescence spectra are shown in Supplementary Fig. 5, with the corresponding parameters shown in Supplementary Table 2. As shown in Supplementary Fig. 5A, peak a is the Rayleigh scattering peak ( $\lambda_{\text{ex}} = \lambda_{\text{em}}$ ); peak b ( $\lambda_{\text{ex}} = 250.0 \text{ nm}$ ,  $\lambda_{\text{em}} = 346.0 \text{ nm}$ ) relates to the spectral characteristic of Trp and Tyr residues; and peak c ( $\lambda_{\text{ex}} = 200.0 \text{ nm}$  and  $\lambda_{\text{em}} = 342.0 \text{ nm}$ ) mainly reveals the fluorescence spectral behavior of polypeptide backbone structures. From the results, it was clearly observed that both fluorescence peaks b and c of BSA had been quenched with the addition of C3G. The decrease in fluorescence intensity of the two peaks and the analysis of

fluorescence characteristics of the peaks revealed that the interaction between C3G and BSA might induce slight unfolding of the polypeptides of BSA and some microenvironmental and conformational changes in it (Zuo et al., 2015). The three-dimensional fluorescence spectra of Hb and Mb are shown in Supplementary Fig. 5. Peak a is the Rayleigh scattering peak ( $\lambda_{\text{ex}} = \lambda_{\text{em}}$ ), and Peak b and c mainly displays the spectral feature of Tyr and Trp residues. After the addition of C3G, the fluorescence intensity of the three peaks decreased but to different degrees. Therefore it concluded that there were specific interactions occurring between C3G and Hb or Mb, indicating that C3G had complexed with Hb or Mb to

**Table 3**

Docking results of C3G with BSA, Hb and Mb by using the Autodock program generated different ligand conformations.

Protein	Rank	$\Delta G$ (kcal/mol)	$E_{\text{intermol}}$ (kcal/mol)	$E_{\text{VHD}}$ (kcal/mol)	$E_{\text{elec}}$ (kcal/mol)	$E_{\text{total}}$ (kcal/mol)	$E_{\text{torsional}}$ (kcal/mol)
BSA	1	−8.13	−9.32	−9.18	−0.15	−1.31	1.19
	2	−8.04	−9.24	−9.02	−0.21	−1.12	1.19
	3	−7.89	−9.08	−8.99	−0.1	−1.09	1.19
	4	−7.89	−9.08	−8.93	−0.15	−1.48	1.19
	5	−7.61	−8.8	−8.5	−0.3	−1.92	1.19
	6	−7.59	−8.79	−8.48	−0.31	−2.03	1.19
	7	−7.54	−8.74	−8.84	0.1	−1.82	1.19
	8	−7.47	−8.66	−8.77	0.11	−1.84	1.19
	9	−7.41	−8.6	−8.69	0.09	−1.88	1.19
	10	−6.58	−7.77	−7.84	0.07	−1.95	1.19
Hb	1	−5.99	−7.18	−7.15	−0.03	−1.51	1.19
	2	−5.94	−7.13	−7.07	−0.06	−1.6	1.19
	3	−5.93	−7.12	−7.21	0.1	−1.58	1.19
	4	−5.92	−7.11	−7.07	−0.04	−1.52	1.19
	5	−5.91	−7.11	−7.04	−0.06	−1.57	1.19
	6	−5.89	−7.09	−7.02	−0.06	−1.59	1.19
	7	−5.88	−7.07	−7.04	−0.03	−1.57	1.19
	8	−5.86	−7.06	−6.99	−0.07	−1.54	1.19
	9	−5.45	−6.64	−6.65	0.01	−1.3	1.19
	10	−5.29	−6.49	−6.42	−0.06	−2.09	1.19
Mb	1	−7.78	−8.97	−8.98	0.01	−1.02	1.19
	2	−7.49	−8.69	−8.71	0.03	−0.65	1.19
	3	−7.19	−8.39	−8.2	−0.19	−1.16	1.19
	4	−7.1	−8.3	−8.2	−0.1	−1.1	1.19
	5	−7.08	−8.27	−8.07	−0.2	−1.15	1.19
	6	−7.08	−8.27	−8.21	−0.06	−1.14	1.19
	7	−6.94	−8.13	−7.98	−0.14	−1.13	1.19
	8	−6.9	−8.09	−8.13	−0.03	−1.83	1.19
	9	−6.58	−7.77	−7.61	−0.16	−1.4	1.19
	10	−5.72	−6.91	−6.62	−0.29	−1.77	1.19

change its microenvironment and conformation (He et al., 2014). We speculated C3G could form a complex with BSA, Hb or Mb, and change its microenvironment and conformation, which agrees with the static quenching mechanism. Besides, we observed that the Rayleigh peak intensity of Mb increased after the addition of C3G, which indicated that electronically coupled occurred between Mb and C3G.

### 3.7. CD spectra

Besides fluorescence spectra, CD spectroscopy is another powerful method to analyze the effects of C3G on the secondary structure of proteins (Shi et al., 2012). The CD spectra and the relevant data of BSA, Hb or Mb are shown in Fig. 2. As shown in the results, the spectra of BSA, Hb and Mb have two negative bands at 208 and 222 nm, which are characteristic of  $\alpha$ -helical structures in protein. After the addition of C3G, the CD signal of BSA, Hb and Mb decreased markedly, indicating that the binding interaction of C3G with BSA, Hb or Mb induced changes in the secondary structures of the protein (Liu, Tian, Tian, Hu, & Chen, 2004). While the CD spectra of proteins are similar before and after conjugation, it is obvious that the structure of protein–C3G is still predominately  $\alpha$ -helix (Xie et al., 2014). With the help of the CDNN program, the secondary structural elements of pure BSA, Hb or Mb and its conjugate system were calculated. The results are listed in the Fig. 2. As shown in Fig. 2, the  $\alpha$ -helix content of free BSA was 63.8%. When C3G was added to the BSA solution, the  $\alpha$ -helix contents of BSA increased. The increase of the  $\alpha$ -helix percentage of C3G–BSA showed that the addition of C3G would intensify the protein skeleton. We deduced the reason for this was that the interaction with C3G has weakened the solvation effect between BSA and the water molecules, causing the side chains of BSA to associate, increasing the  $\alpha$ -helix percentage. For Hb and Mb, the  $\alpha$ -helix contents after the addition of C3G were decreased. We conjectured the  $\alpha$ -helix conformation of Hb and Mb partially changed into  $\beta$ -sheet,

$\beta$ -turn and random coil structures. Furthermore, it suggested that the binding of C3G to Hb and Mb could result in the loosening of the structure of protein, which might result from a break in the hydrogen bonding networks of proteins (Zuo et al., 2015). In a word, the variation in the contents of  $\alpha$ -helix implied that the binding interactions of C3G with BSA, Hb or Mb partially induced the environmental changes of BSA, Hb or Mb.

### 3.8. Molecular modeling

Molecular modeling was employed as a complementary way to help deepen the understanding of drug–biomacromolecule interaction. From the docking calculation, scores of conformers were picked up from the cluster analysis. Ten possible conformational clusters were obtained from many docking runs for the binding site of C3G with BSA, while the number of conformational clusters of C3G with Hb and Mb were 10, indicating that BSA, Hb and Mb had more than one possible binding sites to bind with C3G. The different kinds of binding energy including the final intermolecular energy ( $\text{vdw} + \text{Hbond} + \text{desolvo energy} + \text{electrostatic energy}$ ) (1), the final total internal energy (2), the torsional free energy (3) and the unbound system's energy (4) were also obtained from the Autodock molecular modeling data. The estimated free energy of binding = (1) + (2) + (3) + (4) (Wang et al., 2014). Table 3 shows the estimated free energy of binding ( $\Delta G$ ), the final intermolecular energy ( $E_{\text{inter-mol}}$ ),  $\text{vdw} + \text{Hbond} + \text{desolvo energy}$  ( $E_{\text{VHD}}$ ), the electrostatic energy ( $E_{\text{elec}}$ ), the final total internal energy ( $E_{\text{total}}$ ), and the torsional free energy ( $E_{\text{torsional}}$ ). From the data in Table 3, we made the following conclusions. Firstly, the values of  $\Delta G$  indicated that formation of complex (BSA–C3G, Hb–C3G and Mb–C3G) were spontaneous, and the sequence was BSA > Mb > Hb.  $E_{\text{VHD}}$  energy (van der Waals energy ( $E_{\text{vdw}}$ ),  $E_{\text{Hbond}}$  and  $E_{\text{desolvo}}$ ) were the main energy, implying that van der Waals and hydrogen bonding forces were the main forces (Faucci, Melani, & Mura, 2002). Furthermore, electrostatic forces ( $E_{\text{elec}}$ ) were also involved in the binding

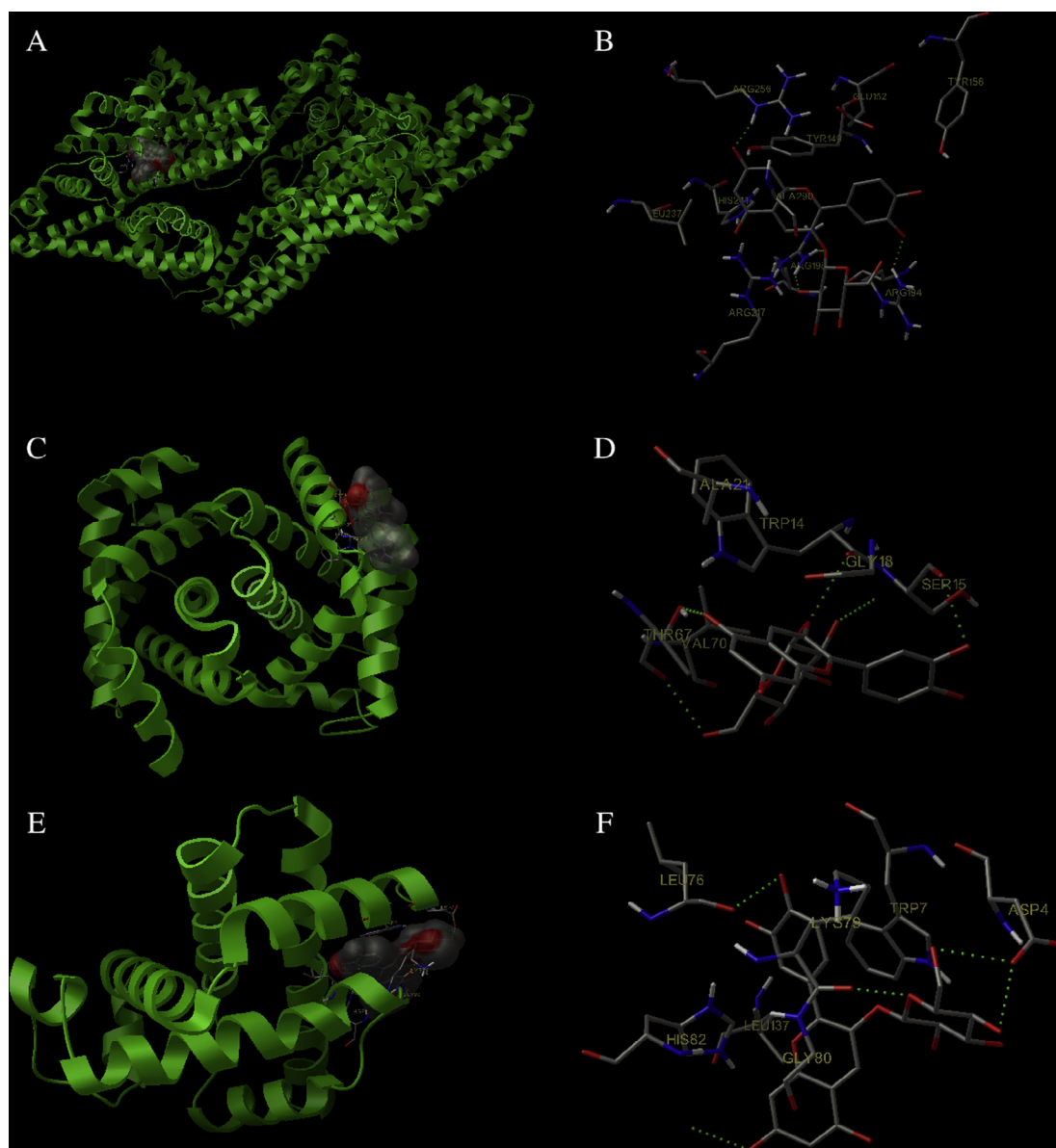


**Fig. 3.** Predicted orientation of the binding conformation of C3G with BSA (A and B), Hb (C and D) and Mb (E and F). (A, C and E) secondary structure of BSA, Hb and Mb around C3G, (B, D and F) hydrogen bond between C3G and BSA, Hb and Mb.

interactions of C3G with BSA, Hb and Mb, but were not the main driving forces, which was in accord with the thermodynamic parameter results.

The best energy ranked results, the nearby amino acid residues and the microenvironment of C3G with BSA, Hb and Mb were also obtained (Fig. 3). As shown in Fig. 3A and B, there were ten amino acid residues that took part in the binding interactions of BSA with C3G. These amino acid residues were Leu-237, Arg-256, His-211, Arg-217, Glu-162, Tyr-149, Ala-290, Arg-193, Arg-194 and Tyr-156. Among above amino residues, Arg, His and Glu were polar amino residues. Therefore, we speculated Van der Waals forces took part in their binding interaction. In addition, four hydrogen bonds (Arg-256, 1.916 Å, Arg-194, 2.233 Å, Arg-198, 1.885 Å and 1.785 Å) were also predicted from the most favorable binding site. Fig. 3C and D showed the predicated binding model of Hb and C3G. The results indicated that six amino acid residues (Val-70, Thr-67, Tyr-14, Ala-21, Gly-18 and Ser-45) were involved in its binding with C3G. The modeled Hb-C3G structure shows that Van der

Waals forces may also be present because of the presence of Thr and Ser, which have a high polarity. In addition, among the above amino acid residues in Hb, Thr-67, Trp-14, Ser-15 and Lys-11 formed hydrogen bonds with the -OH of C3G. The hydrogen bond lengths of them were 1.687 Å, 2.134 Å, 2.186 Å, and 2.968 Å, respectively. Fig. 3E and F shows the predicated binding model of Mb and C3G. There were seven amino acid residues (Leu-76, Leu-137, Lys-79, Tyr-7, Asp-4, His-82 and Gly-80) that took part in the binding interactions of Mb with C3G. The results showed that Van der Waals forces may be present because of the presence of Lys, Tyr, Asp, His and Gly (highly polar). In addition to this, four hydrogen bonds (Asp-4, 2.398 Å, Lys-79, 2.552 Å, Leu-76, 1.852 Å and Leu-137, 3.308 Å) were also predicted from the most favorable binding site. In a conclusion, Van der Waals forces and hydrogen bonding forces were involved in these binding interactions. The computational results were in accordance with the fluorescence experimental results. Furthermore, the heme group in Hb and Mb was near to the binding site of C3G with Hb or Mb. Therefore,



the binding interactions of C3G with Hb or Mb might affect the structure and the exposure of heme groups in Hb and Mb, which was in accordance with the UV–vis experimental results.

### 3.9. The equilibrium of bound and unbound C3G

Free C3G is in equilibrium with protein–C3G as it is transported through the blood. Therefore, the parameters for binding between C3G and proteins must be considered in determining the availability of C3G for transport into cells (Smith, Di, & Kerns, 2010). BSA and Hb are transport proteins in the blood, so we studied the equilibrium of bound and unbound C3G with BSA and Hb. According to the Scatchard model, if the Scatchard plot is a straight line, this could be an indication that all the binding sites have the same affinities and a simple binding reaction occurs. If the plot is curved, it demonstrates that it binds to more than one type of site or if there is co-operativity in binding (Lopes & Kataký, 2012). The Scatchard model was used to calculate the value of  $f_u$ :

$$\frac{r}{[Q]_f} = nK_b - K_b r \quad (11)$$

$$r = \frac{[Q]_b}{[P]} \quad (12)$$

$$f_u = \frac{[Q]_f}{[Q]} \times 100\% \quad (13)$$

$$f_u = \frac{1 - n[P]/[Q] - K_d/[Q] + [(1 + n[P]/[Q] + K_d/[Q])^2 - 4n[P]/[Q]]^{1/2}}{2} \quad (14)$$

where  $r$  represents the number of moles of bound antioxidants ( $[Q]_b$ ) per mole of protein,  $n$  represents the number of binding sites on the protein molecule,  $K_a$  is the binding constant,  $[Q]_f$  is the concentration of free antioxidants, and  $[P]$  is the total concentration of protein.  $[Q]$  is the total concentration of antioxidants.  $K_a$  is the binding constant and  $K_d = 1/K_a$ . The Scatchard plots for C3G which relate the value of  $r/[Q]_f$  to the value of  $r$  for BSA and Hb are shown in Supplementary Fig. 6(A and C). The Scatchard plots were straight, suggesting that C3G could bind independently to a set of equivalent sites on the proteins. So we could use Eq. (14) for the binding parameters. As shown in Supplementary Fig. 6(B and D), it was observed that the concentrations of free C3G for BSA and Hb were  $f_u > 92\%$  and  $f_u > 93\%$ , respectively. Furthermore, the values of  $f_u$  were all increased with increasing C3G concentrations. The results demonstrated that the concentration of free C3G in plasma was enough to be stored and transported from the circulatory system to reach their target sites to provide their therapeutic effects.

## 4. Conclusion

In conclusion, to explore the influence of C3G on proteins *in vivo*, we investigated the binding mechanisms of C3G with BSA, Hb and Mb to obtain important results including the binding constants, binding energy, binding sites, binding forces, etc. We also calculated the equilibrium of bound and unbound C3G with BSA and Hb. The UV–vis results indicated that C3G was able to interact with BSA, Hb and Mb, and made the heme groups exposed in Hb and Mb. In addition, fluorescence and time-resolved fluorescence spectroscopy revealed that the interaction process belonged to a static quenching mechanism and the main forces were Van der Waals and hydrogen bonding forces. Synchronous fluorescence spectroscopy indicated that C3G could change the polarity around the fluorophore molecule and the conformation of Hb. Furthermore, CD, UV–vis, and three-dimensional fluorescence spectra

implied that the secondary structures of three proteins were altered. Moreover, the CD spectra showed that there was a decrease in percentage of  $\alpha$ -helix after the interaction of C3G with Hb and Mb, while that of BSA was increased, supporting the hypothesis that the micro-environment and conformation of BSA, Hb and Mb were changed in the presence of C3G. The results were well supported by molecular modeling analysis. Furthermore, the result of equilibrium fraction showed that the concentration of free C3G in plasma was high enough to be stored and transported from the circulatory system to reach their target sites to provide their therapeutic effects. These results could provide more detailed information to understanding the delivery process of C3G *in vivo*.

## Acknowledgment

We are grateful to the financial support from the Program for Science & Technology of Shandong Province (2008RKA188).

## Appendix A. Supplementary data

Supplementary data associated with this article can be found, in the online version, at <http://dx.doi.org/10.1016/j.foodchem.2015.09.089>.

## References

- Chamani, J., Vahedian-Movahed, H., & Saberi, M. R. (2011). Lomefloxacin promotes the interaction between human serum albumin and transferrin: A mechanistic insight into the emergence of antibiotic's side effects. *Journal of Pharmaceutical and Biomedical Analysis*, 55(1), 114–124.
- Chatterjee, S., & Kumar, G. S. (2014). Targeting the heme proteins hemoglobin and myoglobin by janus green blue and study of the dye–protein association by spectroscopy and calorimetry. *RSC Advances*, 4(80), 42706–42715.
- Chen, H., Ikeda-Saito, M., & Shaik, S. (2008). Nature of the Fe–O<sub>2</sub> bonding in oxy-myoglobin: Effect of the protein. *Journal of the American Chemical Society*, 130(44), 14778–14790.
- Cheng, H., Liu, H., Bao, W., & Zou, G. (2011). Studies on the interaction between docetaxel and human hemoglobin by spectroscopic analysis and molecular docking. *Journal of Photochemistry and Photobiology B: Biology*, 105(2), 126–132.
- Faucci, M. T., Melani, F., & Mura, P. (2002). Computer-aided molecular modeling techniques for predicting the stability of drug–cyclodextrin inclusion complexes in aqueous solutions. *Chemical Physics Letters*, 358(5), 383–390.
- Fleschhut, J., Kratzer, F., Rechkemmer, G., & Kulling, S. E. (2006). Stability and biotransformation of various dietary anthocyanins *in vitro*. *European Journal of Nutrition*, 45(1), 7–18.
- He, W., Dou, H., Li, Z., Wang, X., Wang, L., Wang, R., & Chang, J. (2014). Investigation of the interaction between five alkaloids and human hemoglobin by fluorescence spectroscopy and molecular modeling. *Spectrochimica Acta Part A: Molecular and Biomolecular Spectroscopy*, 123, 176–186.
- Kähkönen, M. P., & Heinonen, M. (2003). Antioxidant activity of anthocyanins and their aglycons. *Journal of Agricultural and Food Chemistry*, 51(3), 628–633.
- Kratz, F. (2008). Albumin as a drug carrier: Design of prodrugs, drug conjugates and nanoparticles. *Journal of Controlled Release*, 132(3), 171–183.
- Li, D., Zhu, J., Jin, J., & Yao, X. (2007). Studies on the binding of nevidensin to human serum albumin by molecular spectroscopy and modeling. *Journal of Molecular Structure*, 846(1), 34–41.
- Liu, J., Tian, J., Tian, X., Hu, Z., & Chen, X. (2004). Interaction of isofraxidin with human serum albumin. *Bioorganic & Medicinal Chemistry*, 12(2), 469–474.
- Lopes, P., & Kataký, R. (2012). Chiral interactions of the drug propranolol and  $\alpha$ 1-acid-glycoprotein at a micro liquid–liquid interface. *Analytical Chemistry*, 84(5), 2299–2304.
- Lu, D., Zhao, X., Zhao, Y., Zhang, B., Zhang, B., Geng, M., & Liu, R. (2011). Binding of Sudan II and Sudan IV to bovine serum albumin: Comparison studies. *Food and Chemical Toxicology*, 49(12), 3158–3164.
- Mahato, M., Pal, P., Kamilya, T., Sarkar, R., Chaudhuri, A., & Talapatra, G. (2010). Hemoglobin–silver interaction and bioconjugate formation: A spectroscopic study. *The Journal of Physical Chemistry B*, 114(20), 7062–7070.
- Molina-Bolívar, J., Galisteo-González, F., Ruiz, C. C., Medina-O, M., & Parra, A. (2014). Spectroscopic investigation on the interaction of maslinic acid with bovine serum albumin. *Journal of Luminescence*, 156, 141–149.
- Noda, Y., Kaneyuki, T., Mori, A., & Packer, L. (2002). Antioxidant activities of pomegranate fruit extract and its anthocyanidins: Delphinidin, cyanidin, and pelargonidin. *Journal of Agricultural and Food Chemistry*, 50(1), 166–171.
- Patel, R., Mir, M. U. H., Maurya, J. K., Singh, U. K., Maurya, N., Khan, A. B., & Ali, A. (2015). Spectroscopic and molecular modelling analysis of the interaction between ethane-1,2-diyl bis (N,N-dimethyl-N-hexadecylammoniumacetoxyl) dichloride and bovine serum albumin. *Luminescence*.

- Ross, P. D., & Subramanian, S. (1981). Thermodynamics of protein association reactions: Forces contributing to stability. *Biochemistry*, 20(11), 3096–3102.
- Seeram, N., Momin, R., Nair, M., & Bourquin, L. (2001). Cyclooxygenase inhibitory and antioxidant cyanidin glycosides in cherries and berries. *Phytomedicine*, 8(5), 362–369.
- Serraino, I., Dugo, L., Dugo, P., Mondello, L., Mazzon, E., Dugo, G., ... Cuzzocrea, S. (2003). Protective effects of cyanidin-3-O-glucoside from blackberry extract against peroxynitrite-induced endothelial dysfunction and vascular failure. *Life Sciences*, 73(9), 1097–1114.
- Shaikh, S., Seetharamappa, J., Kandagal, P., Manjunatha, D., & Ashoka, S. (2007). Spectroscopic investigations on the mechanism of interaction of bioactive dye with bovine serum albumin. *Dyes and Pigments*, 74(3), 665–671.
- Shen, H., Gu, Z., Jian, K., & Qi, J. (2013). In vitro study on the binding of gemcitabine to bovine serum albumin. *Journal of Pharmaceutical and Biomedical Analysis*, 75, 86–93.
- Shi, S., Zhang, Y., Xiong, X., Huang, K., Chen, X., & Peng, M. (2012). The influence of flavonoids on the binding of pantoprazole to bovine serum albumin by spectroscopic methods: With the viewpoint of food/drug interference. *Food Chemistry*, 135(3), 1083–1090.
- Smith, D. A., Di, L., & Kerns, E. H. (2010). The effect of plasma protein binding on in vivo efficacy: Misconceptions in drug discovery. *Nature Reviews Drug Discovery*, 9(12), 929–939.
- Tang, L., Zuo, H., & Shu, L. (2014). Comparison of the interaction between three anthocyanins and human serum albumins by spectroscopy. *Journal of Luminescence*, 153, 54–63.
- Tsuda, T., Horio, F., Uchida, K., Aoki, H., & Osawa, T. (2003). Dietary cyanidin 3-O- $\beta$ -D-glucoside-rich purple corn colour prevents obesity and ameliorates hyperglycemia in mice. *The Journal of Nutrition*, 133(7), 2125–2130.
- Wang, Y.-q., Tang, B.-p., Zhang, H.-M., Zhou, Q.-h., & Zhang, G.-c. (2009). Studies on the interaction between imidacloprid and human serum albumin: spectroscopic approach. *Journal of Photochemistry and Photobiology B: Biology*, 94(3), 183–190.
- Wang, Y.-Q., Zhang, H.-M., & Cao, J. (2014). Binding of hydroxylated single-walled carbon nanotubes to two hemoproteins, hemoglobin and myoglobin. *Journal of Photochemistry and Photobiology B: Biology*, 141, 26–35.
- Xiang, Y., & Wu, F. (2010). Study of the interaction between a new Schiff-base complex and bovine serum albumin by fluorescence spectroscopy. *Spectrochimica Acta Part A: Molecular and Biomolecular Spectroscopy*, 77(2), 430–436.
- Xie, W., Wei, S., Liu, J., Ge, X., Zhou, L., Zhou, J., & Shen, J. (2014). Spectroscopic studies on the interaction of Ga<sup>3+</sup>-hypocrellin A with myoglobin. *Spectrochimica Acta Part A: Molecular and Biomolecular Spectroscopy*, 121, 109–115.
- Xu, J. W., Ikeda, K., & Yamori, Y. (2004). Upregulation of endothelial nitric oxide synthase by cyanidin-3-glucoside, a typical anthocyanin pigment. *Hypertension*, 44(2), 217–222.
- Zhou, X.-M., Lü, W.-J., Su, L., Shan, Z.-J., & Chen, X.-G. (2012). Binding of phthalate plasticizers to human serum albumin in vitro: A multispectroscopic approach and molecular modeling. *Journal of Agricultural and Food Chemistry*, 60(4), 1135–1145.
- Zuo, H., Tang, L., Li, S., & Huang, J. (2015). Combined multispectroscopic and molecular docking investigation on the interaction between delphinidin-3-O-glucoside and bovine serum albumin. *Luminescence*, 30(1), 110–117.